

## ELECTRONIC SUPPLEMENTARY INFORMATION

### Epitaxial Stabilization *versus* Interdiffusion: Synthetic Routes to Metastable Cubic HfO<sub>2</sub> and HfV<sub>2</sub>O<sub>7</sub> from the Core—Shell Arrangement of Precursors

Nathan A. Fler,<sup>a,b</sup> Melonie P. Thomas,<sup>c</sup> Justin L. Andrews,<sup>a,b</sup> Gregory R. Waetzig,<sup>a,b</sup> Oscar Gonzalez,<sup>a</sup> Guan-Wen Liu,<sup>a,b</sup> Beth S. Guiton,<sup>c\*</sup> and Sarbajit Banerjee<sup>a,b\*</sup>

<sup>a</sup>Department of Chemistry, Texas A&M University, 3255 TAMU, 580 Ross St, College Station, Texas 77843, USA.

<sup>b</sup>Department of Materials Science and Engineering, Texas A&M University, 575 Ross St, College Station, Texas 77843, USA.

<sup>c</sup>Department of Chemistry, University of Kentucky, 505 Rose Street, Lexington, Kentucky 40506, USA

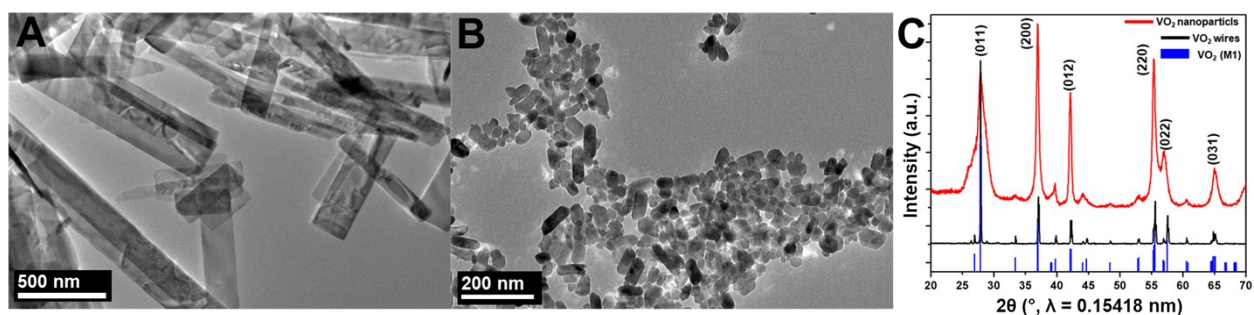
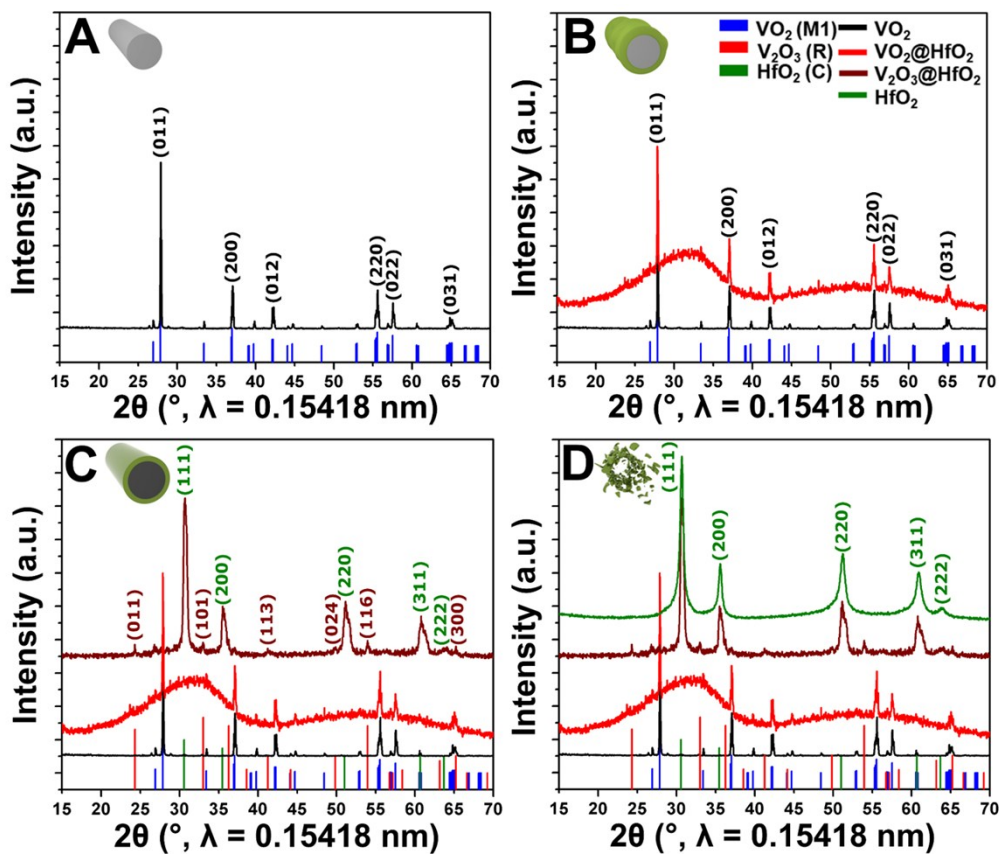
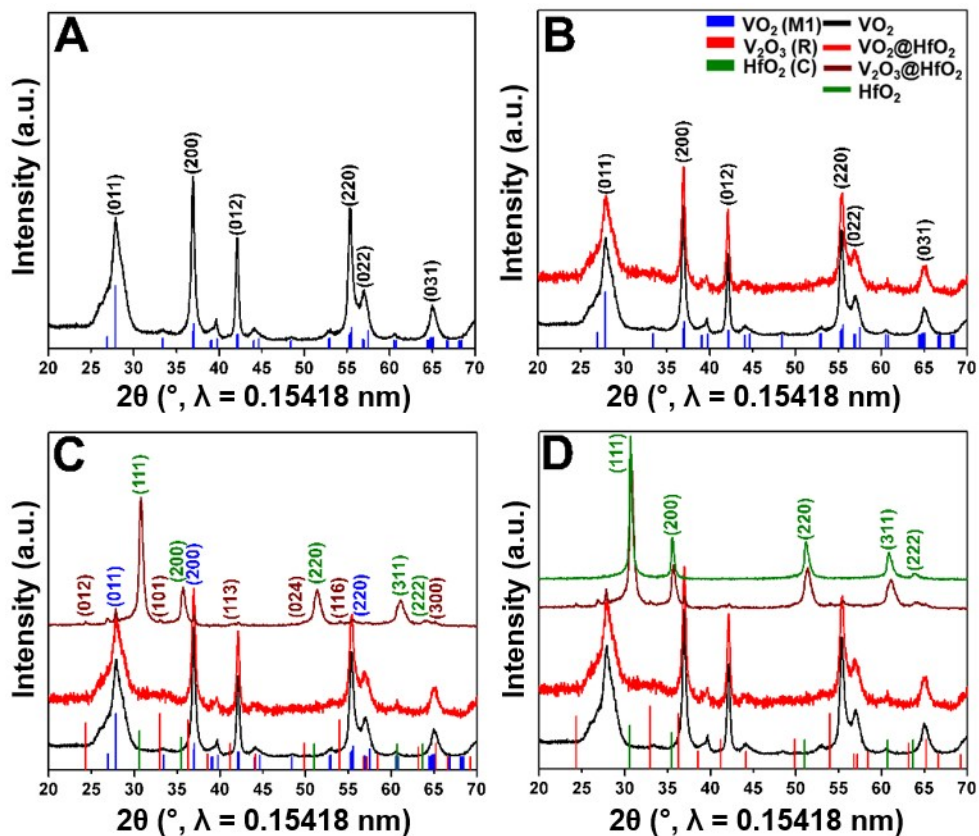


Figure S1: Characterization of VO<sub>2</sub> nanocrystals. TEM images of A) VO<sub>2</sub> nanowires prepared from the hydrothermal reduction of V<sub>2</sub>O<sub>5</sub> by acetone and B) quasi-spherical VO<sub>2</sub> nanocrystals prepared by sol—gel condensation and hydrothermal treatment. C) Powder XRD patterns of VO<sub>2</sub> nanowires (black) and ultrasmall VO<sub>2</sub> nanocrystals (red). The tick marks denote the reflections of the M1 phase of VO<sub>2</sub> (PDF: 43-1051).



**Figure S2:** Indexed powder XRD patterns acquired at room temperature along the synthetic pathway. A) XRD pattern of VO<sub>2</sub> nanowires prepared by acetone reduction of V<sub>2</sub>O<sub>5</sub> (black). B) XRD pattern of VO<sub>2</sub> nanowires coated with an amorphous HfO<sub>2</sub> shell (red). The diffuse scattering background derived from amorphous HfO<sub>2</sub> is clearly apparent. C) Powder XRD pattern acquired subsequent to annealing showing the presence of rhombohedral V<sub>2</sub>O<sub>3</sub> and cubic HfO<sub>2</sub> (maroon). D) Powder XRD pattern after acid etching indicating the stabilization of cubic HfO<sub>2</sub> (green). An indexing and pattern legend is shown in the top right of panel B. The XRD patterns are indexed to the following phases: VO<sub>2</sub> (M1) = 43-1051 and V<sub>2</sub>O<sub>3</sub> (R) = 85-1411.



**Figure S3:** Indexed powder XRD patterns acquired at room temperature along the synthetic pathway. A) XRD pattern of quasi-spherical  $\text{VO}_2$  nanocrystals prepared by sol-gel condensation and hydrothermal treatment (black). B) XRD pattern of quasi-spherical  $\text{VO}_2$  nanocrystals coated with amorphous  $\text{HfO}_2$  shell (red). C) Powder XRD pattern acquired subsequent to annealing showing the presence of rhombohedral  $\text{V}_2\text{O}_3$  and cubic  $\text{HfO}_2$  (maroon). D) Powder XRD pattern after acid etching indicating the stabilization of cubic  $\text{HfO}_2$  (green). An indexing and pattern legend is shown in the top right of panel B. The XRD patterns are indexed to the following phases:  $\text{VO}_2$  (M1) = 43-1051 and  $\text{V}_2\text{O}_3$  (R) = 85-1411.

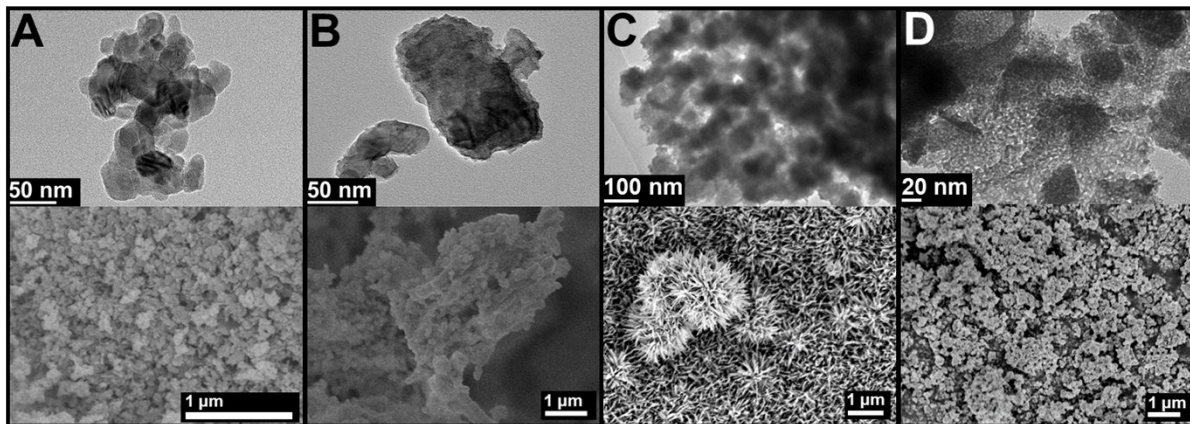


**Figure S4:** TEM and SEM images corresponding to synthetic steps involved in the stabilization of cubic HfO<sub>2</sub>. A) TEM image (top) and SEM image (bottom) of M1-phase VO<sub>2</sub> quasi-spherical nanocrystals. B) TEM and SEM images of quasi-spherical VO<sub>2</sub> nanocrystals coated with an amorphous HfO<sub>2</sub> shell. C) TEM and SEM images of V<sub>2</sub>O<sub>3</sub>@cubic-HfO<sub>2</sub> core—shell structures obtained upon annealing VO<sub>2</sub>@amorphous-HfO<sub>2</sub> structures at 650°C. D) TEM and SEM image of cubic HfO<sub>2</sub> after acid etching of the V<sub>2</sub>O<sub>3</sub> core.

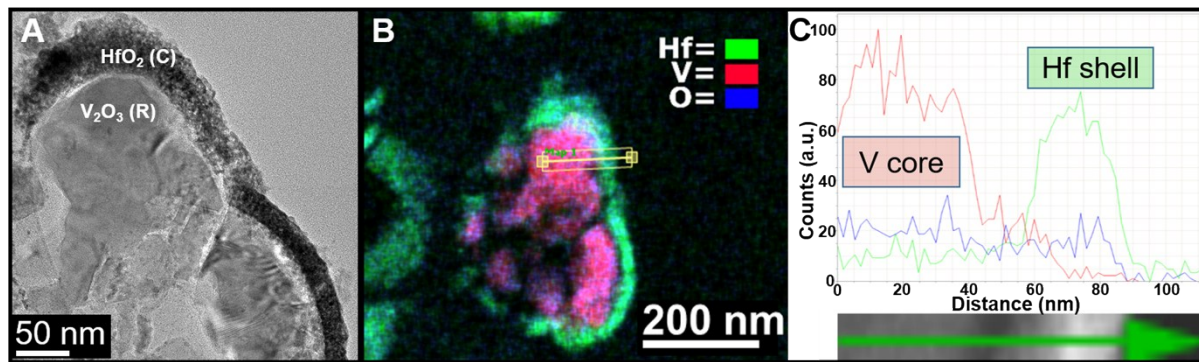


**Figure S5:** Cross-sectional TEM image and EDX line scan of an ultramicrotomed V<sub>2</sub>O<sub>3</sub>@HfO<sub>2</sub> core—shell nanowire. A) Cross-sectional TEM image of a V<sub>2</sub>O<sub>3</sub>@HfO<sub>2</sub> core—shell nanowire; B) corresponding EDX map of the V<sub>2</sub>O<sub>3</sub>@HfO<sub>2</sub> nanowire; and C) EDX line scan along the arrow in panel B. The vanadium signal (red) is highly concentrated within the core, whereas the Hf (green) signal derives predominantly from shell with oxygen (blue) distributed throughout the nanowire.

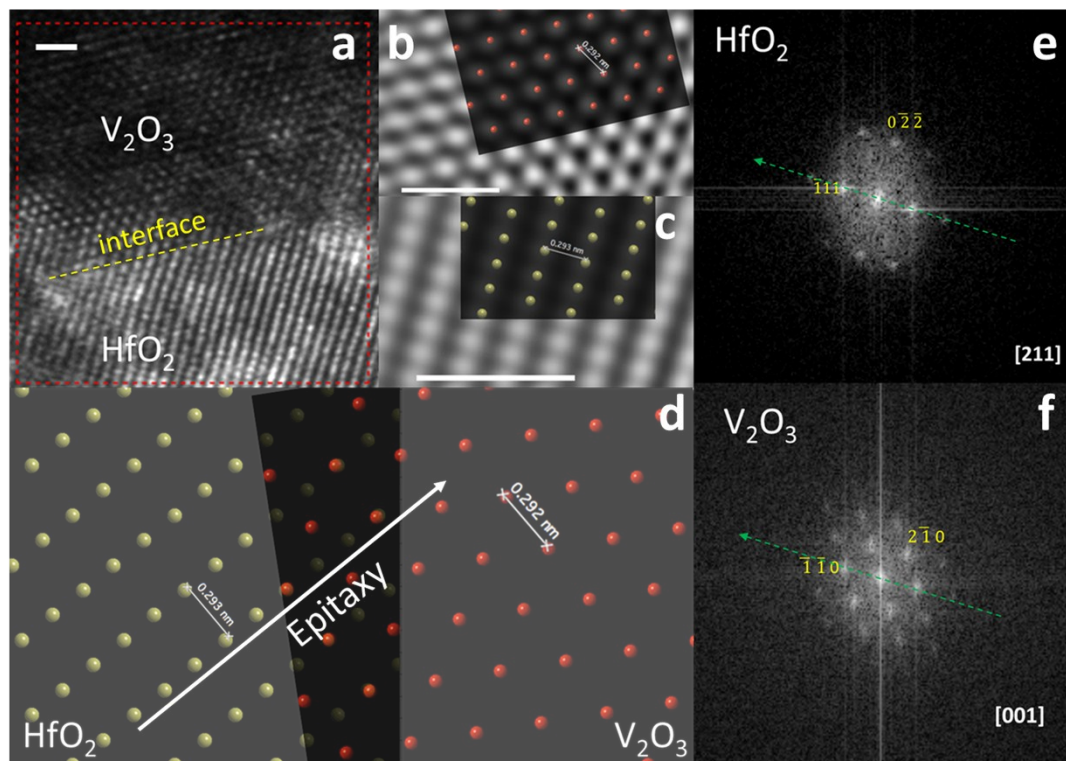


**Figure S6:** The scale bars of (a-c) indicate 1 nm. (a) TEM image of the interface of HfO<sub>2</sub> and V<sub>2</sub>O<sub>3</sub>. (b) and (c) are Fourier filtered TEM images of two interfacial phases, V<sub>2</sub>O<sub>3</sub> and HfO<sub>2</sub>, respectively. The superimposed red and olive color spheres represent V and Hf atoms, respectively. (d) shows the epitaxial direction (white arrow) in the interfacial phases (simulated image from CrystalMaker® software). The FFTs (e and f) obtained from (a) for the two interfacial phases can be indexed to [211] and [001] zone axes of cubic HfO<sub>2</sub> and rhombohedral V<sub>2</sub>O<sub>3</sub>, respectively.

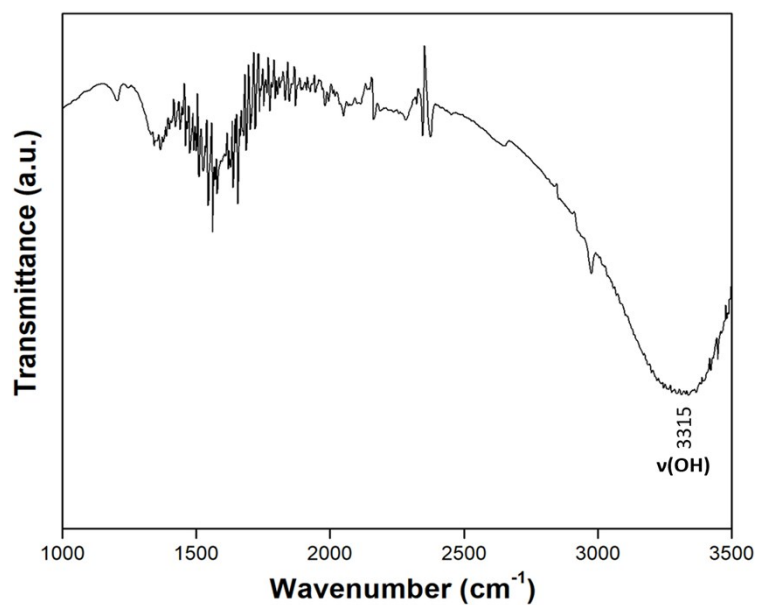


**Figure S7:** FTIR spectrum of cubic HfO<sub>2</sub> after acid treatment. The peak of 3315 cm<sup>-1</sup> reveals the presence of Hf-OH.

Table S1: Rietveld refined values of HfO<sub>2</sub> (C).

HfO <sub>2</sub> (C) // $a/b/c = 5.04793(22)\text{\AA}$ // Space Group = $Fm\bar{3}m$ // $\alpha/\beta/\gamma = 90.0^\circ$ // Vol. = $128.629(16)\text{\AA}^3$						
$\chi^2 = 4.712$		wRp = 6.68%			Rp = 5.08%	
Atom Label	Position	Mult.	x	y	z	Occupancy
Hf	a	4	0.00(0)	0.00(0)	0.00(0)	1.000(0)
O	c	8	0.25(0)	0.25(0)	0.25(0)	1.000(0)

Also shown are fit quality statistics such as the goodness of fit ( $\chi^2$ ), the weighted goodness of fit (wRp) and individual point residuals (Rp). These values demonstrate the high degree of agreement when comparing calculated and observed patterns.